

# A Look into Chaos Detection through Topological Data Analysis

JOSHUA R. TEMPELMAN\* AND FIRAS A. KHASAWNEH†

*Dynamics and Vibration Laboratory, Michigan State University  
Department of Mechanical Engineering, 428 S. Shaw Ln. East Lansing, MI 48824*

---

**Abstract** - Traditionally, computation of Lyapunov exponents has been the marquee method for identifying chaos in a time-series. Recently, new methods have emerged for systems with both known and unknown models to produce a definitive 0/1 diagnostic. However, there still lacks a method which can reliably perform an evaluation for noisy time-series with no known model. In this paper, we present a new chaos detection method which utilizes tools from topological data analysis. Bi-variate density estimates of the randomly projected time-series in the  $p$ - $q$  plane described in Gottwald and Melbourne's approach for 0/1 detection are used to generate a gray-scale image. We show that Wasserstein distances corresponding to the 1-D sub-level set persistence of the images can elucidate whether or not the underlying time series is chaotic. Case studies on the Lorenz and Rossler attractors are used to validate this claim. Similar to the original 0/1 test, our approach is unable to distinguish partially predicable chaotic and periodic behavior in the  $p$ - $q$  space. However, although our method does not deliver a binary 0/1 result, we show that it is able to identify the shift points between chaotic and periodic dynamics in time-series even at high noise-levels.

**Key words.** Topological data analysis | chaos detection | persistent homology | time-series

---

## 1 INTRODUCTION

Chaos is an obscure phenomenon which appears in many physical and theoretical systems. Chaotic systems display a hyper-sensitivity to initial conditions, and their subsequent dynamics are difficult to anticipate as they are seemingly random and sporadic. One famous example of a chaotic system is the Lorenz model [1]. The Lorenz model may be tuned to produce different dynamics i.e. periodic or chaotic as shown by Wernecke *et al.* [2] making it an attractive tool for studying and quantifying chaos.

Differentiating a chaotic time-series from a periodic one is not a trivial task. The traditional recipe for doing utilizes a tangent space method where, for example, the sign of the Maximal Lyapunov Exponent is used to classify the systems behavior. This method has proven reliable, although it is not straightforward to implement for systems with no known model, even with the procedures given by Bennetin [3] and Wolf *et al.* [4]. Recently, Wernecke *et al.* [2] introduced a method which delivers a 0/1 diagnostic for chaos. Like the Lyapunov exponent procedure, this method is reliant on the time-evolution of initially close trajectories. Thus, a known model is required to deliver a diagnosis. Furthermore, this method has not been tested for noise which is inherently present in any experimental data.

A perhaps more popularized emergent method for chaos detection in a time-series was delivered by Gottwald and Melbourne in 2004 [5]. Unlike tangent space methods, no known model is required to perform the 0/1 test. However, it has been shown the method is susceptible to erroneous results in the presence of moderate noise levels [6]. In this paper, we present a new approach for chaos detection that combines elements from the Gottwald and Melbourne method with a tool from Topological Data Analysis (TDA) specifically persistent homology. However, in contrast to the previous work on the 0/1 test, our approach is more robust to noise.

The paper is organized as follows. In Sections 1.1 and 1.2, we introduce the dynamic regimes we are studying and review the 0/1 test, respectively. In Section 2, we describe persistent homology and how this tool can be used in conjunction with prior work on time-series projections to identify the shift point between chaos and periodicity in dynamic systems. Section 3 investigates the robustness of our approach to noise, and the summarizing conclusion is given in Section 4.

---

This material is based upon work supported by the National Science Foundation under Grant Nos. CMMI-1759823 and DMS-1759824 with PI FAK.

Date: April 24, 2022:

\*e-mail: tempelm2@egr.msu.edu

†e-mail: khasawn3@egr.msu.edu

arXiv:1902.05918v2 [nlin.CD] 24 Feb 2019

## 1.1 DEFINITIONS OF THE STUDIED DYNAMIC BEHAVIOR

In the work of Wernecke *et al.* [2], it is shown that the Lorenz system displays periodic, partially predictable chaotic (PPC), and chaotic behavior over a narrow range of a bifurcation parameter. The equations of motion for this classical dynamic system are defined in [1] as

$$\dot{x} = \sigma(y - x), \quad \dot{y} = x(\rho - z) - y, \quad \dot{z} = xy - \beta z. \quad (1)$$

The nominal definitions for the Lorenz constants for this study are  $\beta = 10$ ,  $\sigma = 8/3$ , while  $\rho$  is left as a bifurcation parameter. The manipulation of  $\rho$  can lead to three distinct dynamic regimes as shown in Fig. 1. These regimes are formally defined in [2] as strong chaos (Fig. 1a), partially predictable chaos (Fig. 1b), and laminar flow (Fig. 1c). These regimes will be referred to as chaotic, PPC, and periodic, respectively. The study of the Lorenz system in [2] is successful in identifying the dynamic regime from which the time-series originates using cross-distance scaling and cross-correlations of infinitesimally close trajectories. The results are averaged over 10,000 independent trials to generate a 0/1 diagnostic. However, these evaluations require a known set of differential equations to generate neighboring initial conditions. Thus, the approach in [2] is incapable of detecting chaos in a single time-series originating from systems with unknown models.

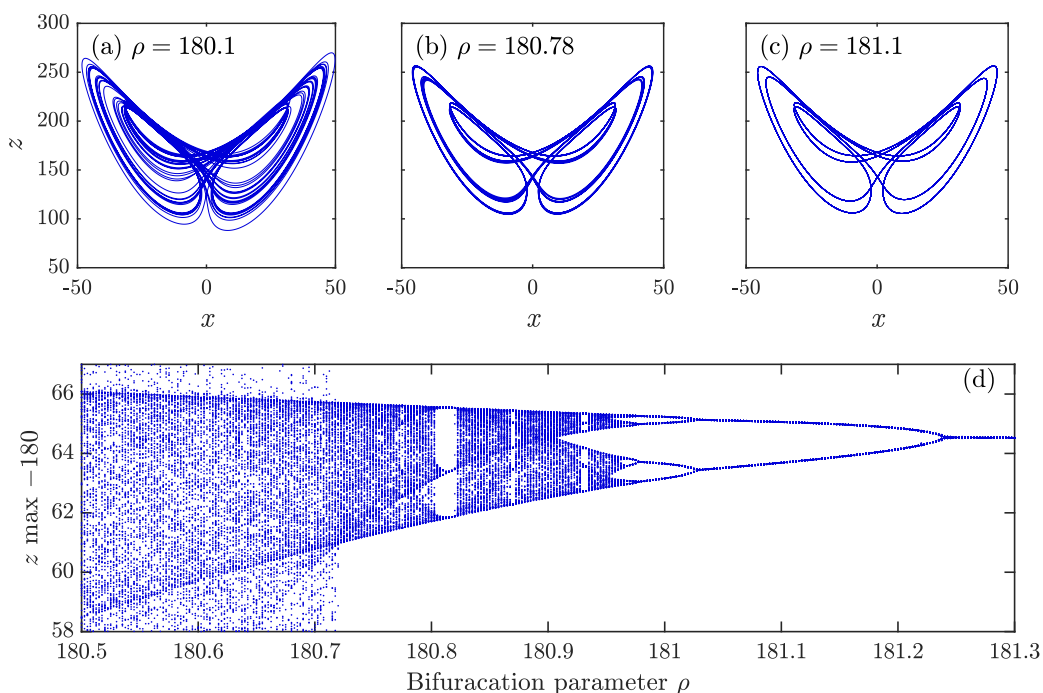


**Figure 1:** The various dynamic regimes displayed by the Lorenz system for modification of the parameter  $\rho$ . A chaotic trajectory is shown in (a) for  $\rho = 180.1$ . PPC is shown in (b) with the trajectory tightly orbiting the attracting braid, and fully periodic behavior is shown in (c) where the trajectory is stable on the manifold. The bifurcation diagram (d) for the parameter  $\rho$  shows chaotic and periodic windows over the bifurcation range of  $\rho \in (180.5, 181.2)$ .

## 1.2 THE TRADITIONAL 0/1 TEST

A 0/1 diagnostic method for identifying chaos in time-series with known or unknown models, i.e. simply using recorded data, is given in [5]. The method has received several updates by Gottwald *et al.* since its original conception [5, 6, 7, 8]. In this paper, we use the version given in the most recent publication on the method [8]. The original test identifies some observable characteristic  $\phi(j)$  of a dynamic system and uses it to construct planar  $(p, q)$  data-sets. These data are constructed, according to [8] with

$$p(n) = \sum_{j=1}^n \phi(j) \cos jc, \quad \text{and} \quad q(n) = \sum_{j=1}^n \phi(j) \sin jc, \quad (2)$$

where  $c$  is a random variable drawn from a uniform distribution in  $(0, \pi)$  and  $n = (0, 1, \dots, N)$ . Using a single data-set of length  $N$ , the number of  $c$  values selected creates  $N_c$  data-sets in the  $(p, q)$  plane. In

this paper,  $N_c = 100$  and  $N = 5000$  unless otherwise stated. The  $p$ - $q$  data is then used to compute the mean-square displacement with

$$M_c(n) = \lim_{N \rightarrow \infty} \frac{1}{N} \sum_{j=1}^N [p_c(j+n) - p_c(j)]^2 + [q_c(j+n) - q_c(j)]^2. \quad (3)$$

Note that in Eq. (3),  $n = (1, 2, \dots, n_{\text{cut}})$  where  $n_{\text{cut}} = N/10$ . In the original 0/1 test, a  $K_c$  value is obtained for each value of  $c$  according to the *regression method*,  $K_c = \lim_{n \rightarrow \infty} \log M_c(n) / \log n$ . Alternatively, it is shown in [7] that a more robust implementation of the test is given by the *correlation method*; the correlation method is used in this paper. To implement this method, begin by defining

$$V_{\text{osc}}(c, n) = (E\phi)^2 \frac{1 - \cos(nc)}{1 - \cos(c)} \quad (4)$$

where  $E\phi$  is the expected value given by

$$E\phi = \lim_{N \rightarrow \infty} \frac{1}{N} \sum_{j=1}^N \phi(j). \quad (5)$$

Now, subtract the  $V_{\text{osc}}$  term from the mean-square displacement to define

$$D_c(n) = M_c(n) - V_{\text{osc}}. \quad (6)$$

Using the standard definitions for covariance and variance respectively

$$\text{cov}(x, y) = \frac{1}{q} \sum_{j=1}^q (x(j) - \bar{x})(y(j) - \bar{y}), \quad \text{and} \quad \text{var}(x) = \text{cov}(x, x), \quad (7)$$

the  $K_c$  value is found using the correlation function

$$K_c = \text{corr}(\xi, \Delta) = \frac{\text{cov}(\xi, \Delta)}{\sqrt{\text{var}(\xi) \text{var}(\Delta)}} \in [-1, 1], \quad (8)$$

where  $\xi = (1, 2, \dots, n_{\text{cut}})$  and  $\Delta = (D_c(1), D_c(2), \dots, D_c(n_{\text{cut}}))$ . The  $K$  value of the time-series is then defined as the median value of the  $K_c$  values with a median near zero noting a periodic time-series and a median near one noting a chaotic time-series.

Although this approach works well in general [7], it is susceptible to yield false results when the data is over-sampled [9] or is injected with substantial noise [6]. An interesting feature of this method is the projection of the data onto the  $p$ - $q$  plane. If the dynamics of the time series is periodic, then the resulting projection will have a regular, typically circular, topology. In contrast, Fig. 2 shows that chaotic dynamics lead to an irregular scattering of points in the  $p$ - $q$  space. Therefore, the topology of the  $p$ - $q$  projections can give insight into the underlying dynamics, as we show in Section 2.

## 2 A TOPOLOGICAL APPROACH

The motivation behind a TDA approach is that data can have shape, and that shape has a meaning. TDA provides tools which lead to a computational summary of the shape of data. We show in Section 2.1 that the 0/1 test given by Gottwald and Melbourne produces data projections with meaningful topology. Therefore, a door is open for quantifying the resulting structure using tools from TDA.

The ability to quantify the topology of a data structure has led to many breakthroughs in various fields. Specifically, TDA has already made meaningful contributions in time series analysis [10, 11, 12], economics [13], machining dynamics [14, 15], biochemistry [16], and plant morphology [17]. In this section, we extend the application of this powerful computational tool to chaos detection.

We use the Lorenz system as a test model for elucidating our TDA-based approach for chaos detection. Three time-series which are generated for different values of the bifurcation parameter in the Lorenz model  $\rho$  are used to produce time-series data which exhibit chaotic ( $\rho = 180.1$ ), PPC ( $\rho = 180.75$ ), and periodic ( $\rho = 181.1$ ) dynamics. The Lorenz time-series generated in this study were produced using the ODE45 function in MATLAB<sup>®</sup> with a relative tolerance of 1e-6, a time step of  $\Delta t = 0.001$ , and a transient cut-off of 100 seconds.

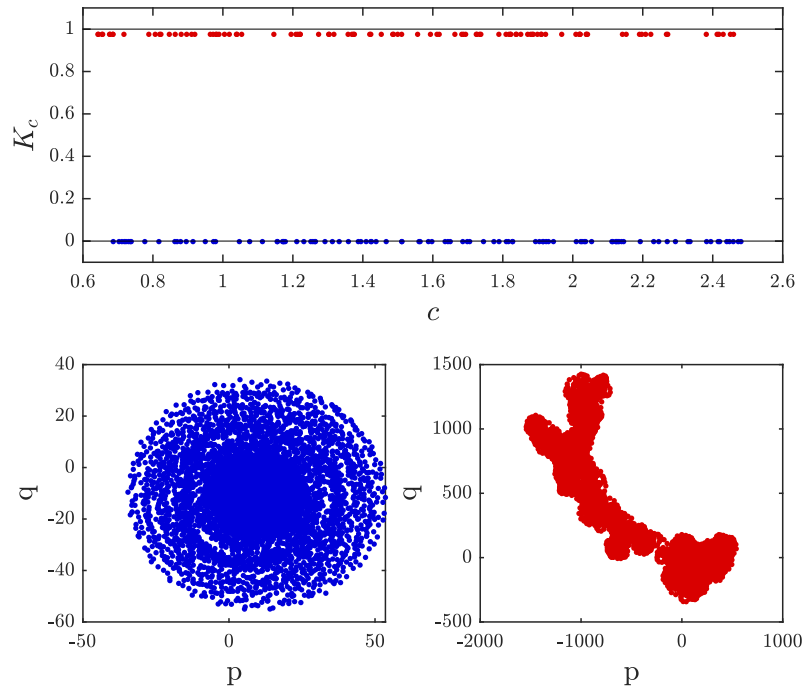


**Figure 2:** (top) the  $K_c$  values found using Gottwald’s method for a periodic time-series (blue) and a chaotic time-series (red). The data is generated with the Lorenz model. (Bottom left) The  $p$ - $q$  projections for the periodic time-series produce a normal, circular geometry. (Bottom right) The  $p$ - $q$  projection of the chaotic time-series produces a scattered, irregular pattern.

Consistent with the original Gottwald method, the generated data is then sub-sampled to mitigate the adverse effects which oversampling may have on the topology of the  $p$ - $q$  projections. This was done using the frequency approach presented by Melosik and Marszalek [9]. This sub-sampling method results in a reconstructed time-series sampled such that  $2f_{\max} < f_s < 4f_{\max}$  where  $f_s$  is the re-construction sampling frequency and  $f_{\max}$  is the maximum significant frequency of the data in the frequency domain. In the original 0/1 test, failure to sub-sample results in false-negatives. Similarly, we found that oversampling contaminates the topological characteristics of the  $p$ - $q$  projections thus leading to incorrect conclusions. As a general rule-of-thumb, it is suggested that the sampling rate chosen in the time-series reconstruction is set to three times the maximum significant frequency of the data.

Our method uses Eq. (2) to generate projections in the  $(p, q)$  plane from time-series data. As shown in the original 0/1 chaos detection tests, a periodic time-series will result in a  $p$ - $q$  set which typically produces an annular geometry while chaotic time-series will display no regular patterns in  $p$ - $q$  space. The regular versus irregular topologies of these data sets make them ideal candidates for the application of TDA via persistent homology.

The subsequent sections give a detailed development of how the TDA approach; the overview is as follows. Multiple projections of  $p$ - $q$  data are generated for a given time series. The bi-variate kernel density estimates of these projections produce a gray scale image (Fig. 4). Sub-level set persistence is then used to provide a computational summary of the topological structure of the data. We give a brief explanation of persistent homology in Section 2.1 and the procedure for applying TDA to the  $p$ - $q$  data in Section 2.2. The consistency of this approach is discussed in Section 2.3, while the results are explained in Section 2.4. A case study on the Rossler system is given in Section 2.4.1. The implementation of this method can be described with Algorithm 1 which is easily implemented using MATLAB<sup>®</sup>.

## 2.1 SUB-LEVEL SET PERSISTENCE

Only a brief explanation of persistent homology, commonly known as persistence, will be provided in this paper. For a more comprehensive explanation of persistence, the reader is directed to [18, 19]. An in depth discussion on the sub-level set persistence method is given by Cohen-Steiner *et al.* [20]. An extensive discussion on filtration is provided in [21] and the formal definitions of homology groups can be found in [22] and [23].

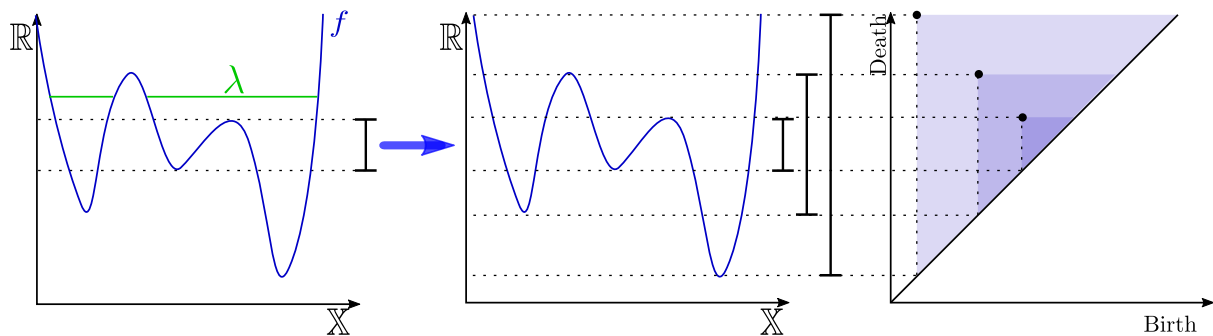


**Figure 3:** An example showing the construction of the 1-D persistence diagram of the function  $f : \mathbb{X} \rightarrow \mathbb{R}$ . (left) The rising “water” level on cross-section cut of a function  $f$  in topological space  $\mathbb{X}$  and (middle) the sub-level sets produced by tracking the “birth” and “death” of topological features on  $f$ . The birth and death times are plotted against on each other (right) to produce the corresponding persistence diagram for the function.

Persistence can be applied to 3-dimensional data such as contour plots or even gray-scaled images. Each point in topological space  $\mathbb{X}$  is assigned some additional dimension which, for the purpose of this explanation, may be thought of as a height coordinate. This represents a real function  $f$  on a topological space  $\mathbb{X}$  with local maxima and minima on the surface. Persistent homology is interested in changes in topology at various *sub-level sets*. For this function  $f : \mathbb{X} \rightarrow \mathbb{R}$ , the  $\lambda$  sub-level set is

$$L_\lambda = \{x : f(x) \geq \lambda\} = f^{-1}([-\infty, \lambda]). \quad (9)$$

For any pair of levels  $\lambda_1 > \lambda_2$  the condition  $L_{\lambda_1} \supseteq L_{\lambda_2}$  must be satisfied and the collection of sets  $\{L_\lambda\}_{\lambda \in \mathbb{R}}$  forms a filtration where the level is the index set [24]. Now imagine a rising water level beginning at the base of  $\mathbb{X}$  and account for each time a new minimum of the surface is touched and new maximum is reached (Fig. 3). As the level  $\lambda$  is raised, new topological features are captured through generators of its homology group. Two dimensions of homology groups are considered. The 0-th groups capture simple connections between components (Fig. 3) while the 1st groups captures regions forming circular structures (Fig. 5).

As new levels are introduced, new generators of homology groups are formed and existing generators conglomerate. The level at which these generates and groupings occur are the *birth* and *death* time, respectively, of the topological feature. Therefore, the three characteristics for each generator are the homology dimension, birth time, and death time. The collection of these points is drawn as what is referred to as a persistence diagram. For  $|D|$  generators, the persistence diagram is  $D = \{(r_j, b_j, d_j) : j = 1, \dots, |D|\}$  where  $r_j$ ,  $b_j$ , and  $d_j$  are homology order, birth time, and death time of the  $j$ th generator [24].

## 2.2 1-D PERSISTENCE OF KERNEL DENSITY ESTIMATES

In this paper, we utilize the 1-D sub-level set persistence to extract the underlying characteristics of the probability densities of the  $p$ - $q$  points. To illustrate the approach, we utilize  $p$ - $q$  projections generated from simulations of the Lorenz system in the periodic, PPC, and chaotic regimes. The bi-variate kernel density estimates (KDEs) are taken of the raw  $p$ - $q$  data according to

$$\hat{f}(x, \mathbf{H}) = \frac{1}{n} \sum_{i=1}^n \mathbf{K}_{\mathbf{H}}(x - x_i), \quad (10)$$

where  $n$  is the number of elements in  $\{x_1, x_2, \dots, x_n\}$  and  $\mathbf{K}_{\mathbf{H}}$  is a smooth function known as the kernel function. Additionally, the density estimates are normalized to have a maximum value of one. The resulting KDEs are converted to a gray scale image and the corresponding sublevel set persistence is computed.

It was found that the most consistent results are obtained when a grid resolution of  $2^5 \times 2^5$  is used. Further, to circumvent sharp peaks from distorting the results, a Gaussian 2-D image filtering function given by

$$G_\sigma = \frac{1}{2\pi\sigma^2} e^{-\frac{x^2+y^2}{2\sigma^2}} \quad (11)$$

must be used, and we set  $\sigma$  to 1.5 for all trials. Should a grid of higher resolution be used, we suggest using a higher  $\sigma$  value, though it should be noted that increasing grid the resolution will drastically lengthen

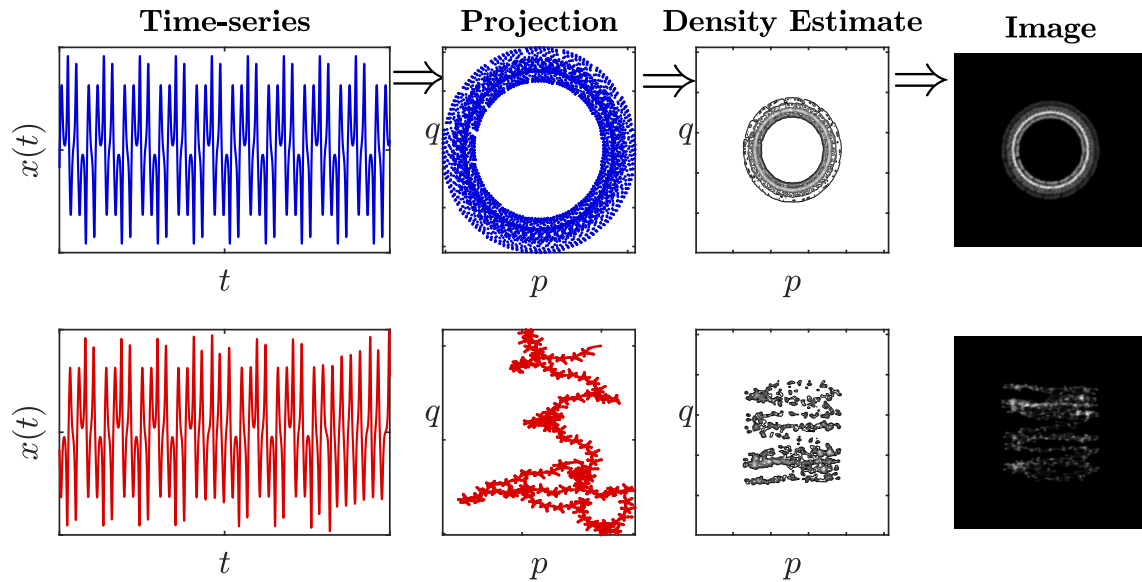


**Figure 4:** The transformation from time-series data to a gray-scaled image. The raw-time series (left) are projected into the  $p$ - $q$  plane (middle-left) before a bi-variate kernel density estimate produces a smooth topological surface (middle-right). The density estimates are then turned into gray-scale images (right) for sub-level set persistence. Shown here is one iteration for laminar flow (top) and chaos (bottom).

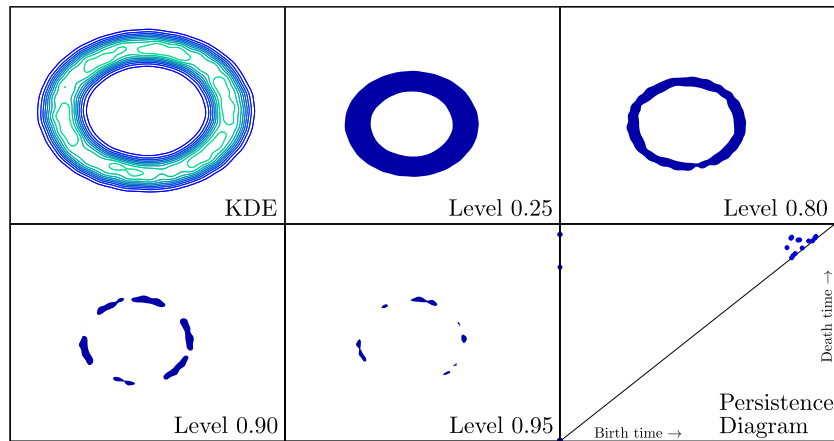


**Figure 5:** Sub-level filtrations for the KDE (left) of a  $p$ - $q$  projection for a periodic time series and the resulting persistence diagram for the 1-st dimension homology groups

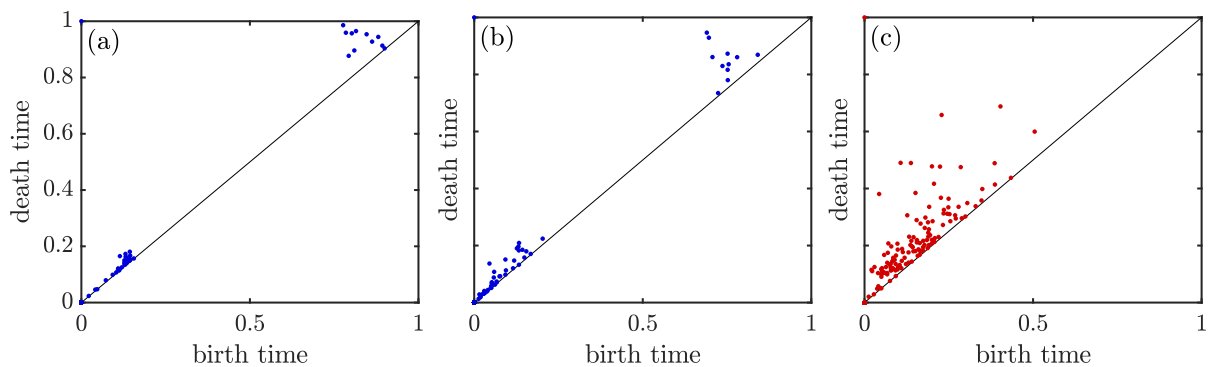


**Figure 6:** (a) A sub-level set persistence diagram constructed for a gray-scaled imaged based on the bi-variate kernel density of a  $p$ - $q$  projection of a periodic time series ( $\rho = 181.1$ ). The same analysis is shown for (b) a  $p$ - $q$  set based on a PPC time series ( $\rho = 180.78$ ) and for (c) a  $p$ - $q$  set based on a chaotic time series ( $\rho = 180.1$ ). The diagrams here are of an image grid resolution of  $2^5 \times 2^5$  with no Gaussian smoothing

the run time of the program. The DIPHA<sup>1</sup> library was used to generate the persistence diagrams and we only use the 1-D persistence. A typical result of the sub-level set persistence is displayed in Fig. 6 for a periodic, PPC, and chaotic time-series for gray scaled images with no Gaussian smoothing. A typical persistence diagram shows a trend of high-birth time with high-death time clusters for the periodic and PPC time series and a randomly dispersed distribution of birth and death times near the diagonal for chaotic time-series. When the persistence is utilized on the gray-scale images as-is (i.e. no pre-filtering of the image), then clusters of low birth/death times appear towards the lower-left of the persistence diagrams. These low birth/death clusters do not give meaningful information about the systems behavior. Nevertheless, this effect is easily mitigated using the 2-D image filter in Eq. (11) (see Fig. 8 for the corresponding persistence diagram).

### 2.3 CONSISTENCY OF THE TOPOLOGICAL APPROACH

Because the  $p$ - $q$  projections depend on the set of randomly sampled  $c$  values, multiple sets of  $p$ - $q$  data can be extracted for each time-series. This is advantageous because it generates multiple  $(p, q)$  projections from a single data set. Because the samplings of the  $p$ - $q$  data are dependent on the random  $c$  values, it is unlikely for two  $p$ - $q$  projections to be identical. Their general structure, however, is hypothesized to be consistent with that of  $p$ - $q$  sets generated from other time series in the same dynamic regime (i.e. periodic, PPC, or chaotic). There are occasions where the  $p$ - $q$  sets are indistinguishable regardless of the underlying dynamics. Therefore, a more robust TDA based diagnostic is obtained by taking the statistical average of multiple realizations.

Specifically, to qualitatively evaluate the consistency of the sub-level set persistence results, three hundred projections of the  $p$ - $q$  data were generated for each respective dynamic regime (periodic, PPC, and chaotic). These projections were then conditioned with the pipeline described in Section 2.1 and the corresponding 1-D sub-level set persistence diagrams were computed. A distance matrix can be constructed to reveal the likelihood of the sub-level persistence being able to discriminate between the different dynamic regions. The  $q$ -Wasserstein distance function [25]

$$W_\infty(X, Y) = \left[ \inf_{\eta: X \rightarrow Y} \sum_{x \in X} \|x - \eta(x)\|_\infty^q \right]^{1/q} \quad (12)$$

where  $\eta$  ranges across all bijections of  $X \rightarrow Y$  is then used to compute a distance matrix for the whole collection of persistence diagrams. In this study, we set  $q = 2$  and used the Hera<sup>2</sup> library to compute the pairwise distances.

	(g)	(h)	(i)
Periodic	0.1737 ±0.08704	0.1503 ±0.0556	0.282 ±0.1066
	(d)	(e)	(f)
PPC	0.1503 ±0.0556	0.1168 ±0.06647	0.264 ±0.1141
	(a)	(b)	(c)
Chaotic	0.282 ±0.1066	0.264 ±0.1141	0.2841 ±0.08274
	Periodic	PPC	Chaotic

**Figure 7:** The Wasserstein distance matrix between persistence diagrams constructed from periodic, PPC, and chaotic time-series. The different regions on the diagram mark the different combinations of persistence diagrams used to calculate distance. The combinations are (a) chaotic and periodic, (b) chaotic and PPC, (c) chaotic and chaotic, (d) periodic and PPC, (e) PPC and PPC, and (g) periodic and periodic, and the resulting matrix is symmetric.

These distances are important because they are deemed stable [20], i.e. small perturbations in the underlying data produce small changes in the persistence diagrams [25]. Fig. 7 shows the resulting distance matrix groups of persistence from the same regime. This grouping also coincides with similar dynamic behavior in the underlying data. To highlight these similarities, in Fig. 7, the average pairwise distances for each region of the distance matrix (i.e. region (a), (b) . . . , (g)) are superimposed on each region. The

<sup>1</sup><https://github.com/DIPHA/dipha>

<sup>2</sup><https://bitbucket.org/greynarn/hera>

averages show that periodic time series result in persistence diagrams which align with other persistence diagrams corresponding to periodic as well as PPC time series since the average Wasserstein distances between these is lower than that of their chaotic counterpart. In contrast, chaotic based persistence diagrams have higher distances when compared to both other chaotic and periodic/PPC persistence diagrams. Thus, it is deduced that the 1-D persistence of the KDE of the  $p$ - $q$  points can distinguish periodic and PPC data from chaotic. However, similar to the original 0/1 test our approach does not differentiate PPC from periodicity (see Fig. 7).

## 2.4 RESULTS AND DISCUSSION

The central motivation for this study is to yield a reliable interpretation of the underlying dynamics of time-series data using persistence. To better understand how this may be achieved, refer to Fig. 8. Here, the persistence diagrams of 500 projections of periodic data along with 500 projections of chaotic data are overlaid. Unlike the persistence diagrams displayed in Fig. 6, the diagrams of Fig. 8 show the persistence diagrams for gray-scale images constructed with a  $2^5 \times 2^5$  grid with Gaussian filtering (Eq. (11)). Notice that the persistence of smoothed images results in an array of birth/death combinations on or very near to the vertical line at birth = 0. This is a result of the filter’s tendency to blend shades thus creating a smooth gradient throughout the image. Recalling the brief description of sub-level set persistence (see Section 2.1), a smoothed gradient will obviously result in a feature being “born” very early and dying much later. Nevertheless, these features reveal little information for discerning the dynamics of the original time series.

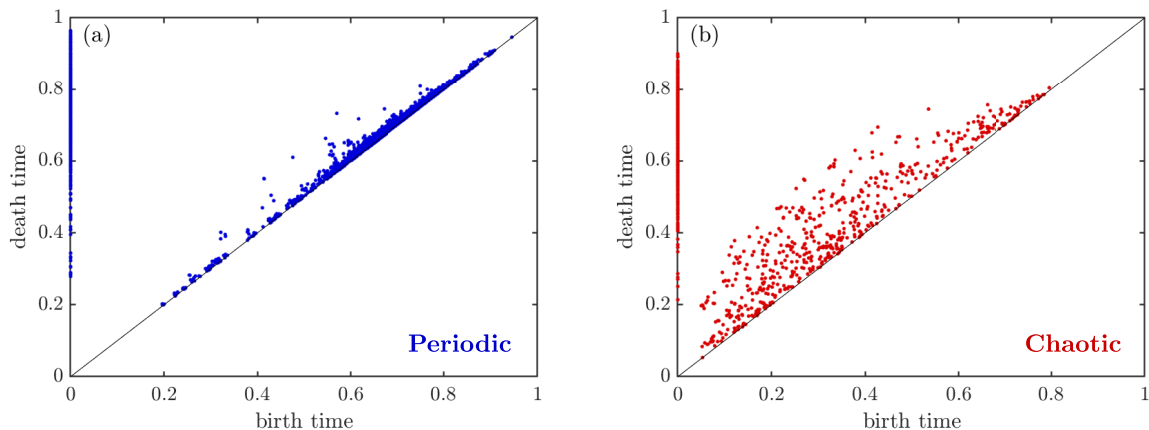


**Figure 8:** 500 persistence diagrams overlaid on one-another generated from image renditions of the density estimates of  $p$ - $q$  projections generated with the Lorenz model for (a) a periodic time-series and (b) a chaotic time-series. The congregation of points along or very near to the zero birth time vertical is clearly seen for both the periodic and chaotic time-series. Aside from this negligible phenomenon, the periodic time-series shows a definitive clustering along or near the diagonal, typically at higher birth/death times while chaotic time-series result in a random and uncluttered birth/death time assortment.

**Observations:** Aside from the clustering of points around a birth time of zero, the persistence diagrams generated from periodic data produce birth/death combinations which are clustered tightly to one-another and bounded to regions on or near the diagonal. Furthermore, these points all appear to be occurring at higher birth and death times than what is seen for their chaotic counterparts. In contrast, the birth/death combinations of persistence diagrams generated from chaotic data do not show any sort of trend, clustering, or bounding. The chaos based persistence diagrams are visually distinguishable from periodic when many trials are overlaid as shown in Fig. 8. Thus, the hypothesis to test is whether or not this behavior may be reliably used to trace back the dynamics of the original time series.

**Classification methods:** As mentioned in section 2.3, the practically unique  $c$  values allow for infinitely many projections of  $p$ - $q$  data for a given time series. Thus, it is feasible to generate multiple  $p$ - $q$  realizations for the given time-series and use a statistical summary of birth and death times to deduce the original dynamics of the time series. In this section, the dispersion of the points as well as the mean distance of persistence data from the diagram origin are used to discern the underlying dynamics of the persistence diagrams.

**Dispersion relations:** The dispersion of the persistence data can give meaningful clues regarding the underlying dynamics. Specifically, defining the *lifetime* of a point to simply be the difference between the birth time and death time, the standard deviation of the resulting lifetimes can give an indication of



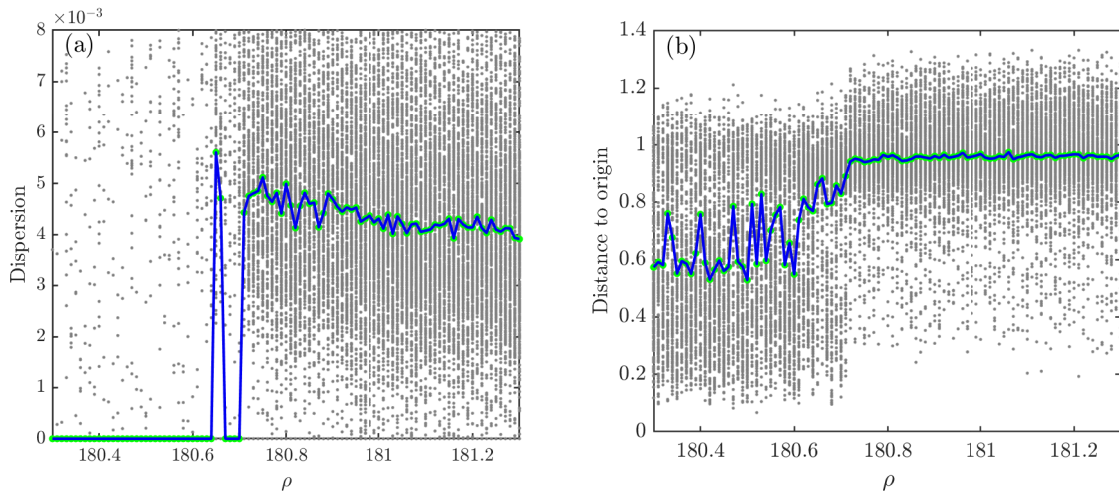


**Figure 9:** Graphical representation of persistence data looking at (left) dispersion and (right) distance from the origin. The images were smoothed by Gaussian filtering and the data used for the statistical summary ignores points with birth times less than 0.01. The gray dots show all points recorded for at the respective bifurcation value. The green dots and blue line correspond to the median value.

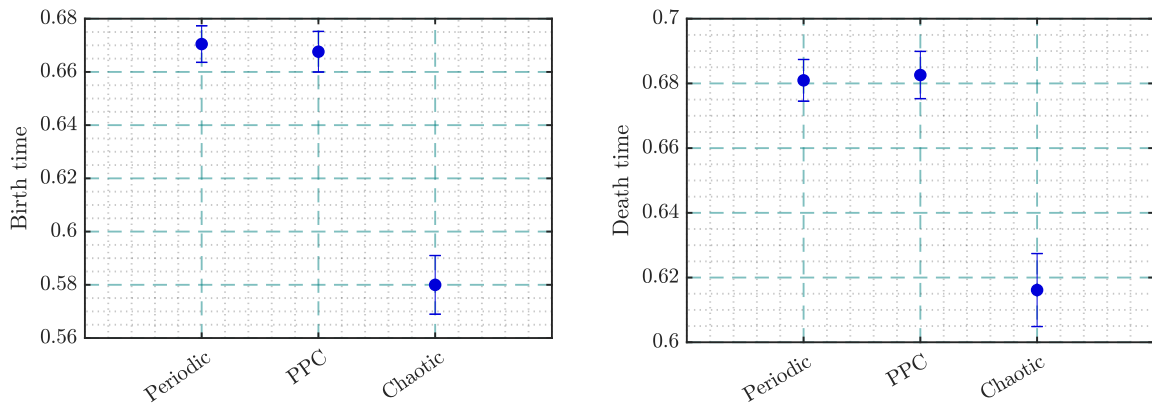


**Figure 10:** Basic statistical summary of 500 persistence diagrams taken from the gray-scaled image renditions of the KDE of the  $p$ - $q$  projections for (left) birth times and (right) death times. The images were smoothed by Gaussian filtering and the data used for the statistical summary ignores points with birth times less than 0.01.

the presence of chaos. Fig. 9a shows that by excluding points with very low birth times (i.e, birth times below 0.01), chaotic time-series will result in persistence diagrams which commonly only have a single remaining point (provided that the data is generated with the same gray-scale image resolution and Gaussian filter as described in this paper). Thus, the dispersion of persistence diagrams corresponding to chaotic data is zero more times than not. The same is not true for periodic time-series where there are commonly multiple lifetimes appearing beyond a birth time of 0.01. If numerous diagrams are generated for each time series (500 are used in Fig. 9), then these trends are exploited by taking the median value of dispersion. The tendency for chaos-based diagrams to yield little to no birth or death times of significance is then exploited, and its median dispersion goes to zero. Thus, the metric here is that a dispersion of lifetime data greater than zero reveals a periodic time-series. While this method performs well for noise free data, it was found to perform very poorly in the presence of noise.

**Mean distance relations:** The threshold for chaotic versus periodic or PPC behavior in persistence diagrams can be defined as a result of the location of the points in the diagram. A basic statistical evaluation of the 500 trials used in Fig. 8 is used to elucidate how such a threshold is defined. Looking simply at the average birth and death times, Fig. 10 shows that the average time of birth and death for periodic data is substantially higher than the chaotic counterpart ( $\approx 0.66$ - $0.68$  for periodic and  $\approx 0.58$ - $0.61$  for chaotic) with several standard deviations separating the means. The statistical summary outlined in Fig. 10 ignores the birth/death combination on or near zero birth time vertical. The statistical summary was conducted by taking the average birth and death time of each diagram and then taking the mean of these average values to deliver one average birth and death time for all of the points on all of

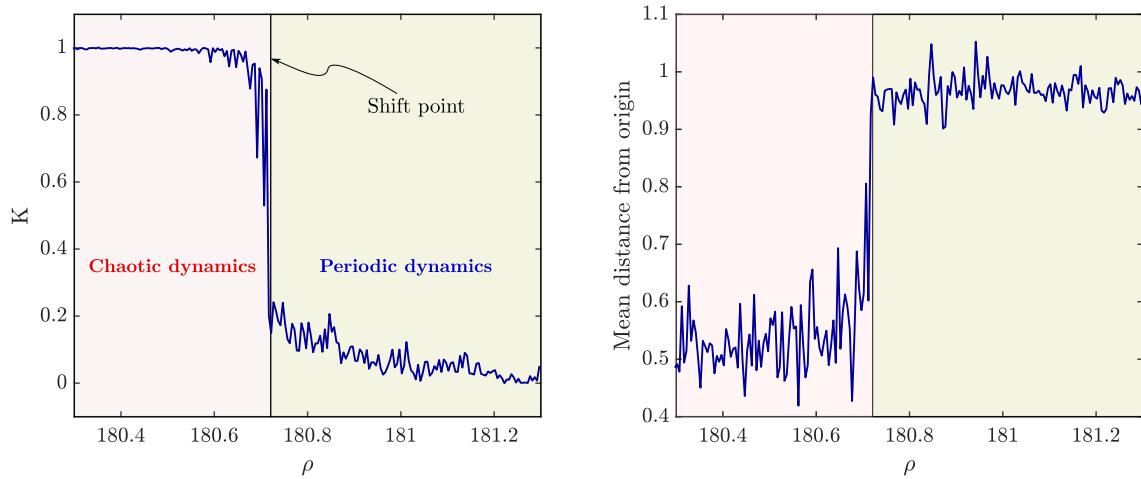


**Figure 11:** A direct comparison of (left) the Gottwald 0/1 test and (right) the proposed method of averaging persistence data based on its position with respect to the origin as applied to Lorenz system times-series over a range of bifurcation parameters. Here, we clearly identify where the dynamics transition from chaotic to periodic.

---

**Algorithm 1** Testing for chaos with persistence

---

```

1: procedure CHAOS( $\mathbf{x}, f_s$ )
2:    $\mathbf{x} \leftarrow$  subsample( $\mathbf{x}, f_s$ )
3:   for  $i = 1:N$  do
4:      $c_i \leftarrow$  rand( $0, \pi$ )
5:      $[\mathbf{p}, \mathbf{q}] \leftarrow f(\mathbf{x}, c)$ 
6:      $\mathbf{P} \leftarrow f(\mathbf{p}, \mathbf{q})$ 
7:      $\mathbf{I} \leftarrow \mathbf{P}$ 
8:      $[\mathbf{B}, \mathbf{D}, \mathbf{d}] \leftarrow$  DIPHA( $\mathbf{I}$ )
9:      $\mathbf{B} \leftarrow \mathbf{B}(\mathbf{d} > 0)$ 
10:     $\mathbf{D} \leftarrow \mathbf{D}(\mathbf{d} > 0)$ 
11:     $\mathbf{s} \leftarrow f(\mathbf{B}, \mathbf{D})$ 
12:     $\mathbf{S}_i \leftarrow$  mean( $\mathbf{s}$ )
13:  end
14:  return mean( $\mathbf{S}$ )

```

$\triangleright$  Time-series data matrix  
 $\triangleright$  Pull one-dimension and sub-sample  
 $\triangleright N \geq 50$  is suggested  
 $\triangleright$  Random  $c$  value  
 $\triangleright$  Project into  $p$ - $q$  space  
 $\triangleright$  Get bi-variate density estimate of  $(p, q)$   
 $\triangleright$  Convert to image  
 $\triangleright$  Call DIPHA and get persistence data  
 $\triangleright$  Cut out persistence data with dimension 0  
 $\triangleright$  Calculate distance from origin for each point  
 $\triangleright$  Take the mean of distances for the diagram  
 $\triangleright$  Compute the mean of all means on index  $i$

---

the diagrams for each data type. The error bars indicate the standard deviations of these average values. Only persistence data with a birth time greater than 0.01 is considered for the statistical summary given in Fig. 10. These modifications to the data are made to sharpen the contrast between diagrams. Thus, it is fair to say that for the Lorenz system, if the average birth or death time of a set of  $p$ - $q$  projections is above 0.64, then the underlying dynamics are periodic. While this method shows how to detect chaos for the Lorenz model, it is later shown in section 2.4.1 that while the general trend holds true, the exact thresholds for each dynamic regime are model specific.

Consistent with the results of Fig. 7, Fig. 10 shows that the persistence diagrams derived from periodic time-series are indistinguishable from those derived from PPC time-series. However, the encouraging result of Fig. 10 is that the birth and death times of persistence diagrams generated with  $p$ - $q$  projections of chaotic time-series are on average lower than their periodic/PPC counterparts. To enhance this separation, the mean distance from the origin is used. With this, the preliminary claim is that if the average distance from the origin falls below 0.9, the original time-series is not periodic. The argument for this threshold is that it is significantly below the mean of distances calculated for persistence diagrams corresponding to periodic/PPC behavior yet significantly above the mean distance calculated for the chaotic counterparts.

Fig. 11 shows a direct comparison between our proposed method (see Fig. 4 and Algorithm 1) and the traditional 0/1 detection test. The results displayed in Fig. 11 are generated using statistical averages of the distances from the origin of persistence data. For each time-series, 50 separate  $p$ - $q$  projections are generated each with a unique  $c$  value. Persistence then gives an array of birth and death times from the gray-scaled rendering of the KDE for each  $p$ - $q$  projection. The mean birth and death time of each

diagram are computed, and then these averages between different  $p$ - $q$  projections are averaged to deliver a single birth and death value for all diagrams constructed with that time-series.

The chaotic versus periodic/PPC regimes established for Fig.11 were obtained using the traditional 0/1 correlation test with the definition that a  $K$  value near zero indicates periodic behavior. When the dynamics are periodic ( $\rho > 180.7$ ), the distance from the origin stabilizes near 0.95. When chaotic dynamics are present, the mean distance falls to a noticeably lower level. Hence, for the case study of the Lorenz model the hypothesis holds true that the statistical summary of persistence data reveals the underlying dynamics of the data.

#### 2.4.1 CASE STUDY: THE ROSSLER SYSTEM

In order for our method to be modular (i.e, applicable to a wide class of signals), it must yield consistent numerical results for periodic and chaotic time-series regardless of the source of the signal. To investigate this, we use the Rossler system to gather additional synthetic data. Like the Lorenz equations, the Rossler model is a classic system which has been studied widely [26] and it is described by

$$\dot{x} = -y - z, \quad \dot{y} = x + ay, \quad \dot{z} = h + z(x - c), \quad (13)$$

where  $a$ ,  $c$  and  $h$  are scalars. The system is leveraged here to compare the behavior of persistence diagrams generated of  $p$ - $q$  projections with the goal of validating the insights gained from studying the Lorenz model. The Rossler data is generated through numerical simulation using the MATLAB<sup>®</sup> ODE45 integration tool with  $\Delta t = 0.01$ , a relative tolerance of  $10^{-5}$ , and a transient cut-off of 1,000 seconds. Three dynamic regimes are shown in Fig. 12 as the bifurcation parameter  $a$  is varied. The parameters selected for this study,  $a \in [0.33 \ 0.557]$ ,  $b = 2$ , and  $c = 4$ , have been shown to provide the desired bifurcation behavior [27]. The bifurcation diagram is provided to serve as a ground-truth for the dynamics of the system. This diagram shows the chaotic regions and the periodicity windows for different values of  $a$ .

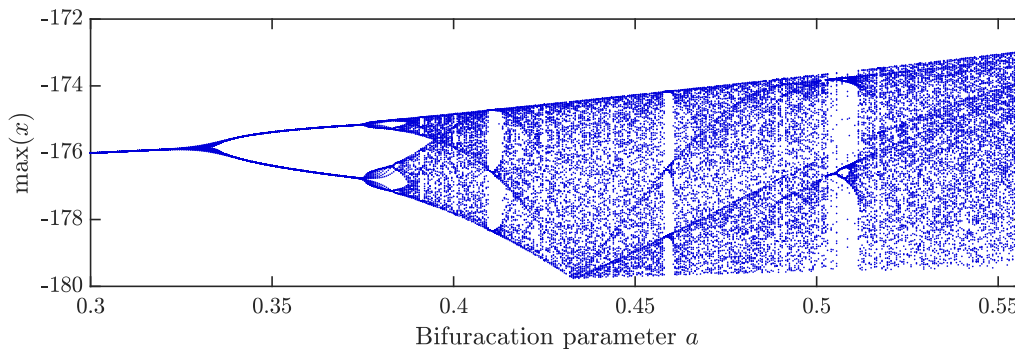


**Figure 12:** Bifurcations of the Rossler system.

The same TDA based approach we used for the Lorenz system for chaos detection is applied to the Rossler data; Time-series were generated for a span of bifurcation parameters, and then they were projected into the  $p$ - $q$  space. The 1-D sub-level set persistence then generated the birth/death times for gray-scale renditions of the KDE of these projections which were smoothed per Eq. (11) with  $\sigma = 1.5$ . The standard 0/1 test as described in [8] is conducted on the time-series generated in the Rossler bifurcation range as well in order for comparison with the topological approach. Fig. 14 shows that the traditional 0/1 chaos test does not always yield a value close to 1 even for regions where seemingly chaotic behavior is produced. Similarly, the mean distance from the origin of birth/death combinations is lower than what was seen for the chaotic Lorenz time-series. The qualitative trend of birth/death combinations for persistence diagrams generated from data with periodic origins which was first seen in the Lorenz model in Fig. 8 is seen again in Fig. 13 for the Rossler system. The birth/death points appear, in general, in locations on or very near to the diagonal of the diagram. In contrast, the clustering is not shown for diagrams constructed for data with chaotic origins.

Fig. 14 shows that while the standard 0/1 test appears to readily identify the periodic time-series as non-chaotic, the median  $K_c$  values are rather ambiguous for time-series generated beyond  $a = 0.4$ . In contrast, the topological approach produces stable results for the chaotic time series, i.e, the mean birth/death times of chaos-based data sets are close to the origin. Thus, it can be concluded from the study of the Rossler system that, similar to the original 0/1 test, two periodic trajectories may not produce identical

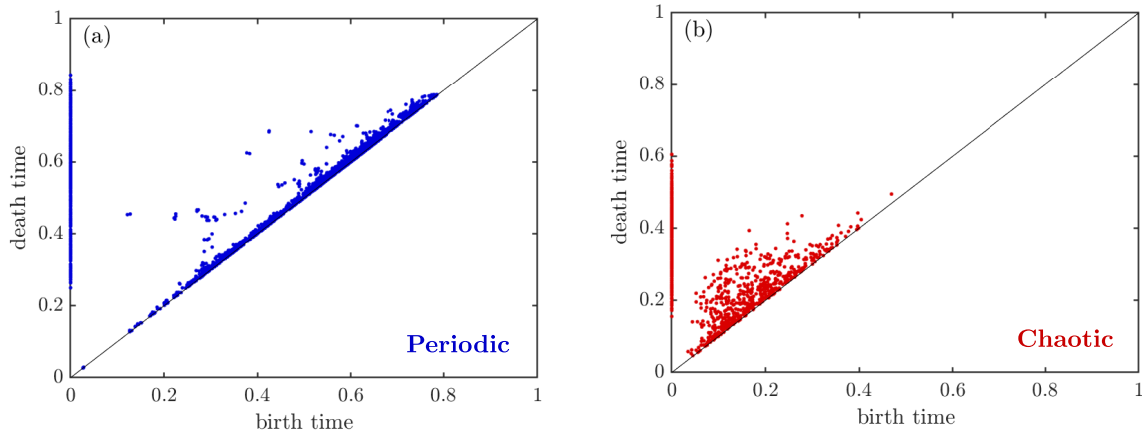


**Figure 13:** 500 persistence diagrams overlaid on one-another generated from image renditions of the density estimates of  $p$ - $q$  projections for a) a periodic time-series and (b) a chaotic time-series constructed with the Rossler equations. The congregation of points along or very near to the zero birth time vertical is again clearly seen for both the periodic and chaotic time-series. The data presents itself in similar clusters to the persistence data constructed with the Lorenz system (Fig. 8), though with lower birth and death times.

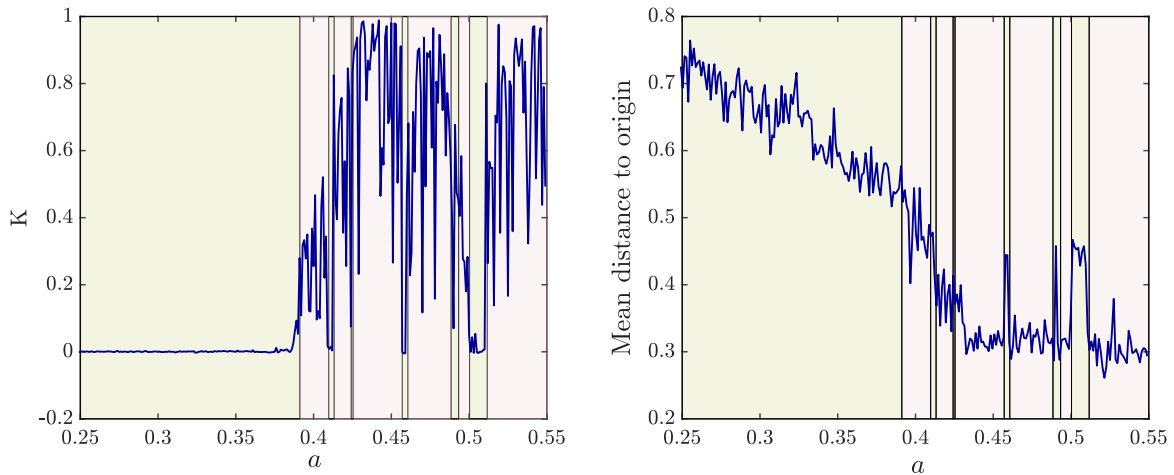


**Figure 14:** (left) The median  $K_c$  values and (right) the mean distance from the origin of a persistence diagram for the time-series constructed with the Rossler equations as the bifurcation parameter  $a$  is varied.

results from the TDA approach. While there is a “gray area” introduced with the results of the study on the Rossler system, Fig. 14b shows the emergence of elevated plateaus in the mean distance to the origin of the persistence diagram for  $a > 0.38$ . These values coincide with windows of periodicity in the bifurcation diagram.

What this means is that tracking the locations of birth and death times with respect to the diagrams origin will not deliver a definitive 0/1 chaos result if only one time series is provided. What this process is capable of, however, is identifying the *shift point* between periodic and chaotic behavior in time-series. If a system is studied across a span of dynamical ranges, then the TDA approach will identify where those shifts occur. Furthermore, Section 3 shows that it can do so at higher noise levels than current methods.

Of course, this metric has its drawbacks, and it is clear from Figs. 11 and 14 that at times the topological approach will give results which contradict what the traditional 0/1 test gives. The original 0/1 test on the Lorenz and Rossler models give  $K$  values which agree with ground-truths found in their respective bifurcation diagrams. The same is true in general for the TDA approach. However, the transition from chaotic to periodic behavior is less obvious than what it is for the original 0/1 test (Fig. 14). Additionally, there are unexpected spikes in the mean persistence distance levels for data generated from chaotic Lorenz time-series (Fig. 11), though the results stabilize once the bifurcation parameter enters the periodic range.

This limitation leaves room for the interpretation of the results rather than delivering a binary result. Nevertheless, this method presents a promising first look into how this powerful computation tool may be used to progress the field of time-series analysis.

### 3 ROBUSTNESS TO NOISE

All of our results thus far have addressed simulated, noise free time-series. The ultimate goal of past and recent 0/1 test procedures is to deliver a diagnostic for data obtained from real signals generated through natural or engineered systems. All signals obtained in the physical world are inherently contaminated with noise to some degree. While tests on clean simulated data are useful, they do not adhere to this standard. Thus, in order for a 0/1 test to be deemed sufficient for real time-series, it must prove itself to be robust to realistic levels of noise.

The effects of noise on the 0/1 test were first discussed in [6] where it was shown that a modified version of the method performs favorably compared to the state-space reconstruction methods [5]. For the noise sensitivity discussion in this paper, the 0/1 test being implemented is the one provided in [7] which was described briefly in Section 1.2. Although the robustness to noise is shown to be favorable for the Gottwald test in comparison to state space reconstruction methods, false positives emerge from the test when the noise levels are elevated.

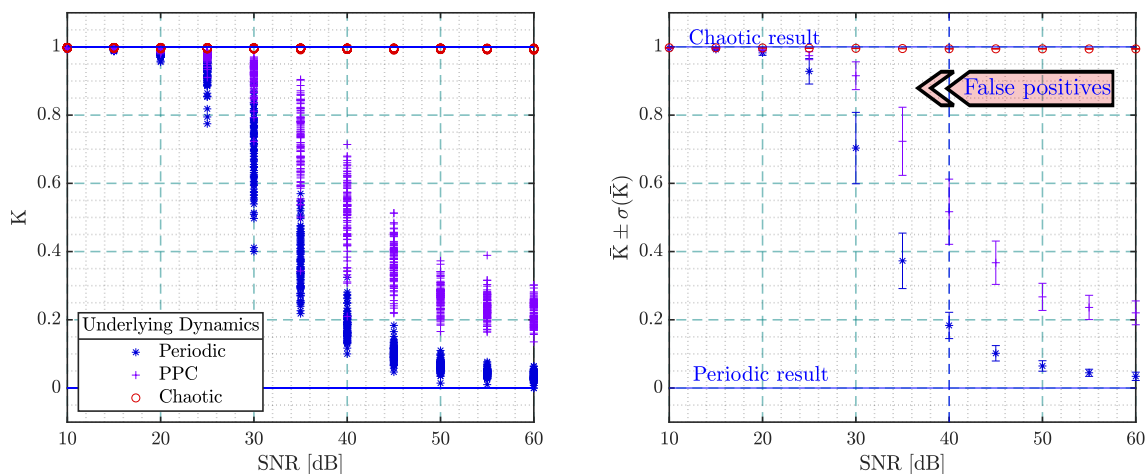


**Figure 15:** Effects of noise on the Gottwald 0/1 chaos test with one-hundred tests being performed for each dynamic regime starting from noise levels of SNR=50dB to SNR=10 dB with all points plotted (left), and a basic statistical summary given (right). It can be seen that noise levels greater than 30 lead to ambiguous results for periodic time-series, and noise levels above SNR = 30 dB lead to false positives.

A brief noise-sensitivity demonstration is given in Fig. 15 to exhibit this for simulations of the Lorenz system. This is done by averaging the median  $K_c$  values for time-series containing signal-to-noise ratios (SNRs) ranging from 60 to 10 decibels (dB). Low noise levels (i.e. high SNR) do not affect the resulting K score of the 0/1 test. However the same is not true for lower SNR levels. At an SNR level of 40 dB, the test begins to yield an ambiguous (non-binary) result. Noise levels above an SNR of 30 dB consistently produce a false-positive indicator for periodic time-series. In order to validate the consistency of this behavior, the test is conducted one-hundred times at each noise level.

The effect of noise on the 0/1 test is mitigated with the topological approach. The reason that a topological evaluation is more robust is because of its ability to emphasize the main features of a data set and ignore minor perturbations [20]. In other words, the general shape of data does not change in the presence of moderate noise; only during a close-up evaluation of time-series data is moderate noise blatantly obvious. The Gaussian smoothing of the images created from the  $p$ - $q$  projections deters noise as well while preserving the main topological features. Only once noise levels reach the point at which the topology of the  $p$ - $q$  projections are no longer recognizable as being derivatives of periodic or chaotic data does the topological approach break down. Nevertheless, the topological approach bolsters a vast improvement to noise robustness than what is seen for the median  $K_c$  values of the 0/1 test. Thus, the topological approach is less prone to producing erroneous results when applied to experimental data.

As the noise levels rise, Fig. 16 shows that the mean distances of the birth/death times from the origin of the persistence diagram randomize. Consequently, Fig. 16 shows that the correlation of a high

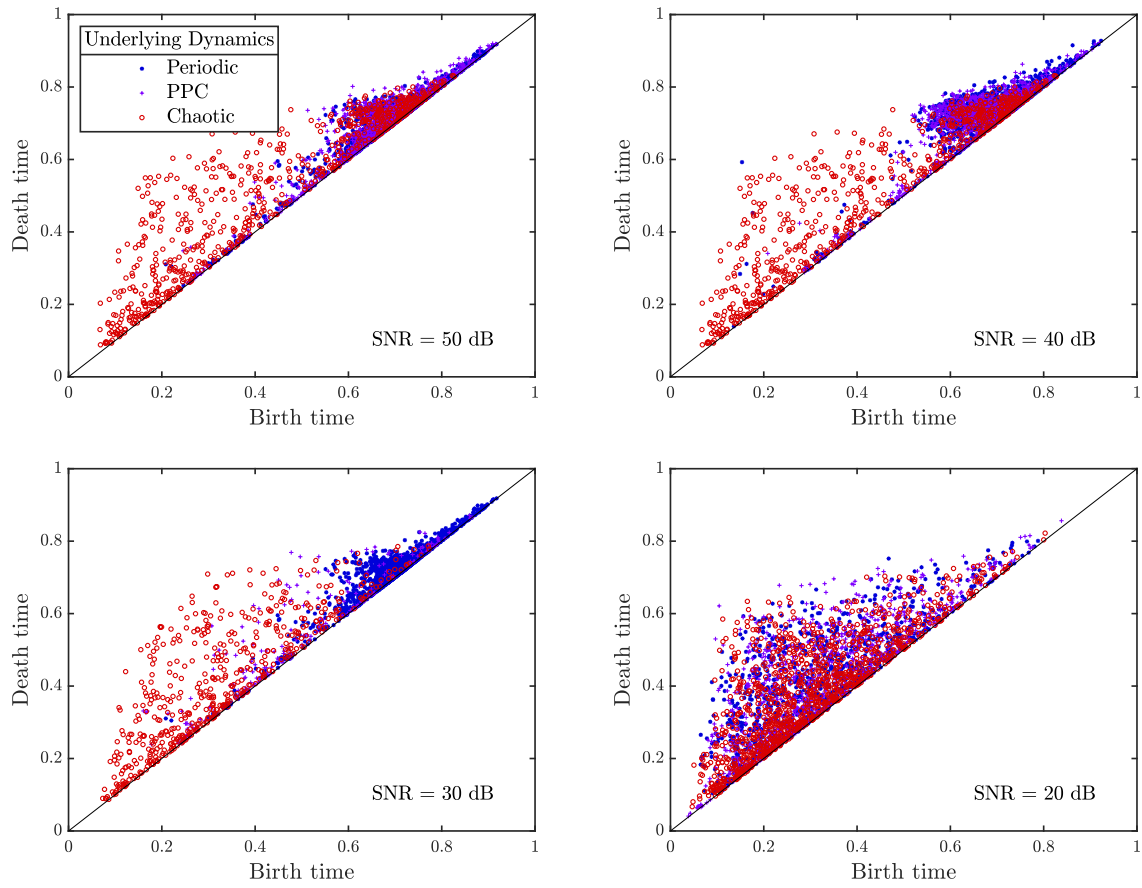


**Figure 16:** The shifts in birth and death time trends as noise is added to the original time series. Shown here is the effect of the noise levels of (a) SNR = 50 dB, (b) SNR = 40dB, (c) SNR = 30 dB, and (d) SNR = 20 dB. The diagram representing each noise level is composed of 500 trials overlaid on one-another with the green markers indicating the birth/death times for data generated from a chaotic time-series and the dark-pink and light-pink markers indicating the birth/death times for data generated from a respective PPC and periodic time series.

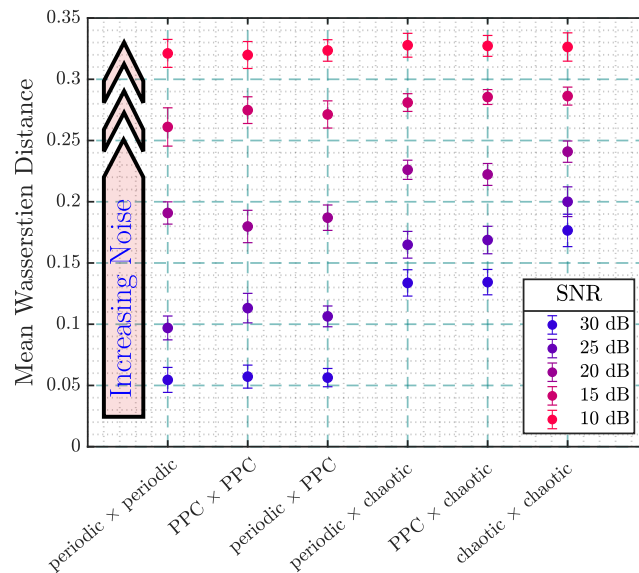


**Figure 17:** The mean distances between persistence diagrams generated from gray-scaled images taken from the density estimates of projections for various noise levels. These distances indicates the ability of the TDA approach to discriminate dynamics at various noise levels. Only once the noise levels are sufficiently high, such as an SNR of 20, does the TDA approach fail to discriminate between time-series.

birth/death time to a periodic time-series dissolves as a result. The mean distances between the diagrams constructed at various noise levels are also studied and the statistical summary is presented in Fig. 17. To do this, fifteen distance matrices were constructed, each of size  $300 \times 300$ , and the average distance and standard deviation of distance for the points in the same dynamic region (i.e, (a), (b), ... (c) from Fig. 7). Fig. 17 shows that there is significant separation between TDA's perception of the  $p$ - $q$  projections generated from periodic versus chaotic time-series for noise-levels beyond the threshold of validity of the original 0/1 test. Specifically, the mean distances between periodic and PPC distances remains below 0.2 for SNR down to 20 dB, and they peak at 0.3 for an SNR of 10 dB.

We note that a minimum SNR of 15 dB is often necessary to extract any useful information from a signal. Fig. 18 shows the effects of noise on the respective techniques as the bifurcation parameter of the Lorenz system is progressed. The behavior of the topological approach is not affected by noise levels in the 50 dB to 35 dB SNR range. In contrast, the behavior of the original 0/1 test is adversely affected by this same noise range and it becomes difficult to identify the transition point between periodic and chaotic. Hence, the TDA method is proven to be more robust to noise.

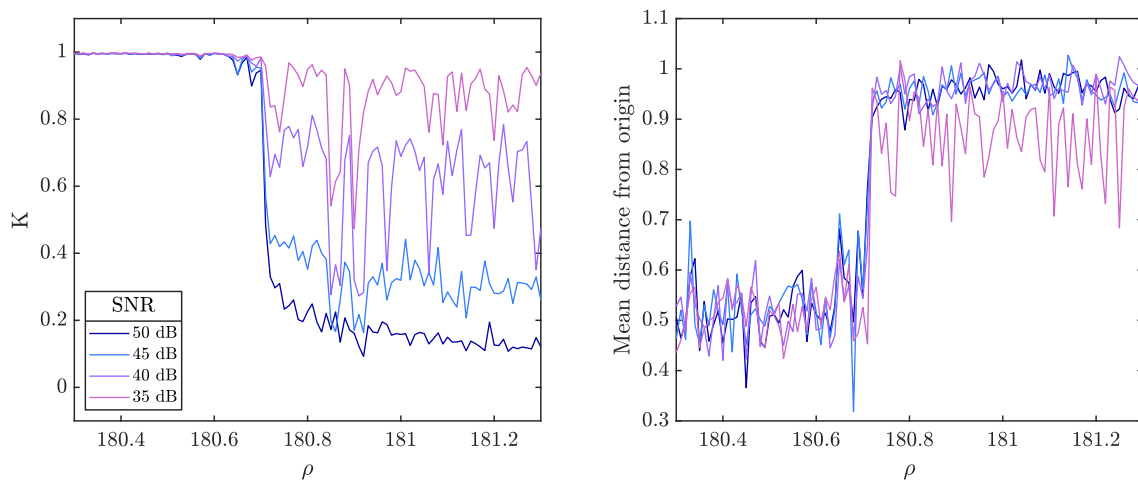


**Figure 18:** The effects of added noise to the Lorenz model. (left) The  $K$  values marking chaotic vs. periodic (1 or 0, respectively). The effects of noise are abundantly clear for noise levels greater than an SNR of 50. Also shown is (right) the results of the topological approach for the same noise levels of the Lorenz system a substantially lesser effect shown for the same noise levels.

## 4 CONCLUSION

The TDA approach presented in this paper and described in Section 2 is shown to detect shifts in the dynamic response using time-series as input. The approach is robust to measurement noise and it yields meaningful results where existing methods fail due to excessive noise. The TDA method is unable to, in the  $p$ - $q$  space at least, to produce a meaningful difference between periodic and PPC [2]. The persistence diagrams produce birth and death times based on unique topological features of the  $p$ - $q$  data. These topological features are exploited to discern whether or not the underlying time-series display chaotic behavior.

Taking the average of the distances for birth/death combinations from the origin of the persistence diagram results in lower distances from the origin for chaos-based persistence trials and higher distances from the origin for trials based on periodic data (Fig. 8). This is shown through the test-scenario of analyzing the Lorenz system across several bifurcation values (Fig. 11). A similar analysis of the Rossler system followed similar trends (Fig. 13), but with different numeric outputs (Fig. 14). Thus, it is concluded that the averaging of birth/death locations may detect the transitions between chaotic and non-chaotic behavior, but it is unable to discern dynamics given just one time-series with no ground-truth.

The dispersion of the persistence data is also studied and it is shown to have meaningful information (Fig. 9). Using Gaussian filtering, the dispersion of persistence data will tend to be zero more times than not should very low birth times (less than 0.01) be excluded from the data. Thus, the median value of a large set of persistence diagrams (500 in this study) will result in a consistent 0/1 result with 0 noting chaotic behavior is present and non-zero dispersion noting periodic time-series data. Although

this approach is attractive because it offers a binary results given just a single time-series, it has very poor robustness to noise and therefore does not offer anything new to the chaos detection methods available.

The main contribution we make with this work is an increase to noise-robustness for chaos detection [20]. The persistence diagrams are resilient to noise, and therefore this approach is as well. The statistical averaging method for birth and death data shows the ability to identify shift points in the dynamics of time-series data at noise levels up to an SNR of 35 (Figs. 15, 17, and 18). This method can be augmented if an additional metric or modification to the procedure would allow for the identification of the systems dynamics by only evaluating one time-series of an unknown system. Although this has not yet been realized, the content of this paper candidly present the results of TDA chaos investigations thus far and lay a firm foundation of work for future research.

**Acknowledgment:** The authors would like to acknowledge Dr. Elizabeth Munch for the helpful insight she provided regarding persistent homology and its applications.

## REFERENCES

- [1] E. N. Lorenz, “Deterministic nonperiodic flow,” *Journal of the Atmospheric Sciences*, vol. 20, pp. 130–141, mar 1963.
- [2] H. Wernecke, B. Sándor, and C. Gros, “How to test for partially predictable chaos,” *Scientific Reports*, vol. 7, apr 2017.
- [3] G. Benettin, L. Galgani, A. Giorgilli, and J.-M. Strelcyn, “Lyapunov characteristic exponents for smooth dynamical systems and for hamiltonian systems: A method for computing all of them. part 2: Numerical application,” *Meccanica*, vol. 15, pp. 21–30, mar 1980.
- [4] A. Wolf, J. B. Swift, H. L. Swinney, and J. A. Vastano, “Determining lyapunov exponents from a time series,” *Physica D: Nonlinear Phenomena*, vol. 16, pp. 285–317, jul 1985.
- [5] G. A. Gottwald and I. Melbourne, “A new test for chaos in deterministic systems,” *Proceedings of the Royal Society A: Mathematical, Physical and Engineering Sciences*, vol. 460, pp. 603–611, feb 2004.
- [6] G. A. Gottwald and I. Melbourne, “Testing for chaos in deterministic systems with noise,” *Physica D: Nonlinear Phenomena*, vol. 212, pp. 100–110, dec 2005.
- [7] G. A. Gottwald and I. Melbourne, “On the implementation of the 0–1 test for chaos,” *SIAM Journal on Applied Dynamical Systems*, vol. 8, pp. 129–145, jan 2009.
- [8] C. H. Skokos, G. A. Gottwald, and J. Laskar, *Chaos Detection and Predictability*, vol. 915. Springer, 2016.
- [9] M. Melosik and W. Marszalek, “On the 0/1 test for chaos in continuous systems,” *Bulletin of the Polish Academy of Sciences Technical Sciences*, vol. 64, pp. 521–528, sep 2016.
- [10] M. Robinson, *Topological Signal Processing*. Springer Berlin Heidelberg, 2014.
- [11] J. A. Perea, “Topological time series analysis,”
- [12] F. A. Khasawneh and E. Munch, “Topological data analysis for true step detection in periodic piecewise constant signals,” *Proceedings of the Royal Society A: Mathematical, Physical and Engineering Science*, vol. 474, p. 20180027, oct 2018.
- [13] M. Gidea, Y. A. Katz, P. Roldan, D. Goldsmith, and Y. Shmalo, “Topological recognition of critical transitions in time series of cryptocurrencies,” *SSRN Electronic Journal*, 2018.
- [14] F. A. Khasawneh and E. Munch, “Chatter detection in turning using persistent homology,” *Mechanical Systems and Signal Processing*, vol. 70-71, pp. 527–541, mar 2016.
- [15] F. A. Khasawneh, E. Munch, and J. A. Perea, “Chatter classification in turning using machine learning and topological data analysis,” *IFAC-PapersOnLine*, vol. 51, no. 14, pp. 195–200, 2018.
- [16] M. Offroy and L. Duponchel, “Topological data analysis: A promising big data exploration tool in biology, analytical chemistry and physical chemistry,” *Analytica Chimica Acta*, vol. 910, pp. 1–11, mar 2016.
- [17] M. Li, M. Frank, V. Coneva, W. Mio, D. H. Chitwood, and C. N. Topp, “The persistent homology mathematical framework provides enhanced genotype-to-phenotype associations for plant morphology,” *Plant Physiology*, p. 001042018, jun 2018.
- [18] J. R. Munkres, *Elements of Algebraic Topology*. WESTVIEW PR, 1993.



- [19] E. Munch, “A user’s guide to topological data analysis,” *Journal of Learning Analytics*, vol. 4, pp. 47–61, jul 2017.
- [20] D. Cohen-Steiner, H. Edelsbrunner, and J. Harer, “Stability of persistence diagrams,” *Discrete & Computational Geometry*, vol. 37, pp. 103–120, dec 2006.
- [21] R. W. Ghrist, *Elementary applied topology*, vol. 1. Createspace Seattle, 2014.
- [22] H. Edelsbrunner and D. Morozov, “Persistent homology: theory and practice,” 2013.
- [23] H. Edelsbrunner and J. Harer, “Persistent homology—a survey,” 2008.
- [24] E. Berry, Y.-C. Chen, J. Cisewski-Kehe, and B. T. Fasy, “Functional summaries of persistence diagrams,”
- [25] M. Kerber, D. Morozov, and A. Nigmatov, “Geometry helps to compare persistence diagrams,”
- [26] O. Rössler, “An equation for continuous chaos,” *Physics Letters A*, vol. 57, pp. 397–398, jul 1976.
- [27] C. Letellier, P. Dutertre, and B. Maheu, “Unstable periodic orbits and templates of the rössler system: Toward a systematic topological characterization,” *Chaos: An Interdisciplinary Journal of Nonlinear Science*, vol. 5, pp. 271–282, mar 1995.